Electronic Supporting Information

Giant Power Factor and High Air-Stability in n-Type Metal-Organic Charge-Transfer Complex

Xiaolei Li,[a, b] Gao Zhang,[a] Xin Zhang,[a] Weitian Zou,[a] Ge Li[b]， Jia Liang,[c] Haijun Wu,[a] Zhen Li,[a] Mingming Zhang,[a] Minqiang Wang,[b] Guanjun Yang*[a] and Chunlei Wan*[c]

[a] State Key Laboratory for Mechanical Behavior of Materials, School of Materials Science and Engineering, Xi'an Jiaotong University, Xi'an, Shaanxi, 710049, China. E-mail: ygj@mail.xjtu.edu.cn

[b] Electronic Materials Research Laboratory, Key Laboratory of Education Ministry, Shaanxi Engineering Research Center of Advanced Energy Materials and Devices, School of Electronic Science and Engineering, Xi ' an Jiaotong University, Xi ' an, Shaanxi, 710049, China.

[c] State Key Laboratory of New Ceramics and Fine Processing, School of Materials Science and Engineering, Tsinghua University, Beijing, 100871, China. E-mail: wancl@mail.tsinghua.edu.cn

1. EXPERIMENTAL PROCEDURES

Materials: All the chemicals were used as received, including $CuBr_2$ (Copper bromide, 99.999%, Sigma-Aldrich), Br-C_6H_4-NH_2 (4-Bromanilinu, 99%, TCI (Shanghai) Development Co. Ltd.), and dimethylformamide (DMF, anhydrous, 99.8%, Sigma-Aldrich). Quartz glasses (JGS1) were purchased from Donghai County Haotian quart glass products Co. Ltd. Indium tin oxide (ITO)/PET (0.125 ± 0.05 mm) were purchased from Ying Kou You Xuan Trade Co., Ltd (China). The (Br-C_6H_4-NH_2)$_2$$CuBr_2$ precursor solution (1.5 mol/L) was formed by dissolving Br-C_6H_4-NH_2 (1032.1 mg) and $CuBr_2$ (670.1 mg) in 2 mL of DMF. Then, the precursor solution was stirred at 60°C overnight.

XRD characterization: Powder X-ray diffraction (XRD) measurements were performed on an Ultima IV X-ray Diffractometer with Cu Kα from 5 to 80° (2θ) at a scanning speed of 0.1 °/s. The calculated XRD pattern was performed using Reflex module package in Materials Studio.

Morphological characterization: SEM tests were performed on a field-emission SEM (MIRA3 TESCAN). High-resolution AFM (INNOVA) was used to test the surface roughness of the (Br-C_6H_4-NH_2)$_2$$CuBr_2$ film.

UV-Vis-NIR spectra characterization: UV-Vis-NIR spectra were measured for Br-C_6H_4-NH_2, $CuBr_2$, and (Br-C_6H_4-NH_2)$_2$$CuBr_2$ by a UV-Vis-NIR Spectrometer (PerkinElmer Lambda 950). Note that double-integrating-sphere mode were used for the measurements of Br-C_6H_4-NH_2 and $CuBr_2$ powders.

ESR spectra characterization: ESR spectra were measured for $CuBr_2$ (25.6mg) and (Br-C_6H_4-NH_2)$_2$$CuBr_2$ (26.5 mg) by an electron spin resonance spectrometer Spectrometer (Bruker EMX PLUS).

Electronic state and band structure characterization: The ultraviolet photoelectron spectroscopy (UPS) were performed in a PHI5000 VersaProbe III (Scanning ESCA Microprobe) spherical capacitive analyzer with a monochromatic He I light source (21.22 eV). The sample bias was −5 V. The X-ray photoelectron spectroscopy (XPS) were performed in an X-ray photoelectron spectrometer (ThermoFisher, ESCALAB 250Xi). X-ray source is a monochrome Al Kα (1486.6 eV) radiation discharge lamp. The XPS spectra were calibrated using the binding energy of C1s (284.8 eV).

Thermoelectric properties characterization: Electrical conductivity, Seebeck coefficient, and thermal conductivity were measured simultaneously from 298 K to 388 K by using Physical Properties Measurement System (PPMS, Quantum Design Inc., San Diego, USA) equipped with the Thermal Transport Option (PPMS-TTO). The TTO option for the PPMS enables measurements of thermal properties, including thermal conductivity κ and Seebeck coefficient S, for sample materials over the entire temperature and magnetic field range of the PPMS. The TTO system measures thermal conductivity by monitoring the temperature drop along the sample as a known amount of heat passes through the sample. TTO measures the thermoelectric Seebeck effect as an electrical voltage drop that accompanies a temperature drop across certain materials. The TTO system can perform these two measurements simultaneously by monitoring both the temperature and voltage drop across a sample as a heat pulse is applied to one end. The PPMS can also measure electrical resistivity ρ by using the standard four-probe resistivity provided by the PPMS AC Transport Measurement System (ACT) option (Model P600). The thermal and electrical connections for an idealized TTO sample are shown in Figure S8.

Here, the four basic physical elements are illustrated in Figure S8: the sample, the epoxy bonds that adhere the leads to the sample, the copper leads, and the heater and thermometer shoe assemblies that screw down onto the

leads. For thermal conductivity and Seebeck coefficient measurements, heat is applied to one end of the sample by running current through the heater ($Q_{+/-}$). The temperatures T_{hot} and T_{cold} are measured at the thermometer shoes. Also during the heat pulse, the Seebeck voltage ($\Delta V = V_+ - V_-$) is monitored. Heat exits the sample to the coldfoot. Electrical resistivity measurements are made both before and after the heat pulse described above. Current ($I_{+/-}$) flows through the sample and the voltage drop across the sample is monitored using the $V_{+/-}$ leads.

The detailed thermoelectric results of the sample tested for 20 times from 298 K to 388 K were shown in Table S1-S7. For the measurements of thermoelectric properties, the area of the samples is 10×10 mm^2. The thickness (~1.4 μm) of the films was determined by Bruker-DektakXT profilometer, as shown in Figure S9. Reliability of measured data has been confirmed by measuring a Ni standard reference sample provided by Quantum Design Inc. The estimated measurements uncertainties are 8% for the electrical conductivity, 6% for the Seebeck coefficient, 11% for the thermal conductivity and 16% for the final figure of merit, *ZT*.

Temperature coefficient of resistance calculation: The temperature coefficient of resistance can be calculated by the equation $R = R_0 [1+\alpha (T-T_0)]$ (R_0 is the resistance at an initial temperature T_0 and R is the resistance at a temperature T °C). The temperature coefficient of resistance of the $(Br\text{-}C_6H_4\text{-}NH_2)_2CuBr_2$ film was extracted from the resistance versus temperature data (see Figure S10).

Computational details： Density functional theory (DFT) calculations were performed by Vienna Ab-initio Simulation Package (VASP).[1, 2, 3] The all-electron projected augmented wave (PAW) potential was used to describe the ion–electron interaction, and Perdew-BurkeErnzerhof (PBE) functional in the framework of generalized gradient approximation (GGA) was used to describe the exchange and correlation function. The energy cutoff of plane wave, Energy and force convergence criteria were set to 520 eV, 1×10^{-6} eV, and 1×10^{-2} eV/Å, respectively. To analyze the behavior and stability in moisture environment, the interaction between water and the $(Br\text{-}C_6H_4\text{-}NH_2)_2CuBr_2$ surfaces were investigated by the ab initio molecular dynamics (AIMD) simulations. The simulations were performed on a 248-atom $(Br\text{-}C_6H_4\text{-}NH_2)_2CuBr_2$ (2×1×1) (011) surface. A vacuum buffer space of 20 Å along the z direction was added to decouple possible periodic interactions. In AIMD simulations, the initial atomic positions were obtained by preheating from 100 K to 300 K for 1 ps as the pre-equilibration. Then the equilibration of 5 ps was performed in the canonical ensemble (NVT ensemble) using Nos´e-Hoover thermostat with 1 fs as a temporal step at the fixed temperature of 300 K.

2. SUPPLEMENTARY TEXT

First way for the calculation of Lorenz number： For most metals, where charge carriers behave like free-electrons, Lorenz number could be estimated as $L_0 = \frac{\pi^2}{3}\left(\frac{k_B}{e}\right)^2 \approx 2.44 \times 10^{-8}$ W Ω K^{-2} for free electrons. For most thermoelectric materials, the real Lorenz number is in fact lower than L_0, depending on the reduced Fermi energy $\xi = E_F/k_BT$ and scattering parameter r.[4, 5] Assuming the main carrier scattering mechanism around room temperature is the acoustic phonon scattering, r could be −1/2. Then the Lorenz number L can be achieved as the following:

$$L = \left(\frac{k_B}{e}\right)^2 \left(\frac{3F_0(\xi)F_2(\xi) - 4F_1^2(\xi)}{F_0^2(\xi)}\right)$$

Where $F_n(\xi)$ represents the Fermi integration,

$$F_n(\xi) = \int_0^\infty \frac{\chi^n}{1+e^{\chi-\xi}} d\chi$$

For a single band approximation, the S can be given as the following:

$$S = \pm\left(\frac{2F_1(\xi)}{F_0(\xi)} - \xi\right)$$

Second way for the calculation of Lorenz number: A satisfactory approximation for L from an experimental S can obtained via the following Equation:[6]

$$L = 1.5 + \exp\left[-\frac{|S|}{116}\right]$$

where L is in 10^{-8} W Ω K^{-2} and S in μV/K.

3. SUPPLEMENTARY DATA

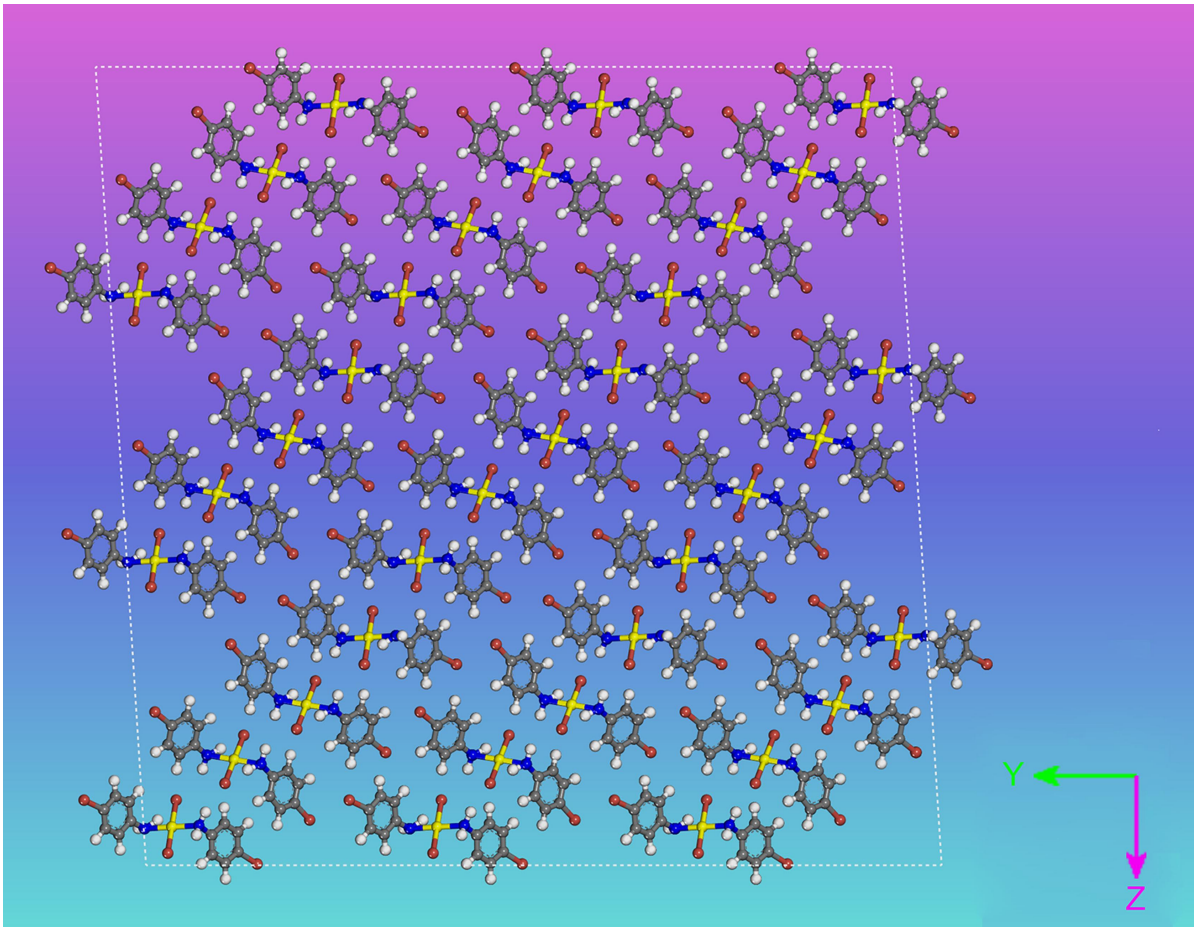

Fig. S1 The packing structure of the $(Br\text{-}C_6H_4\text{-}NH_2)_2CuBr_2$ (3×3×3) from X-axis view.

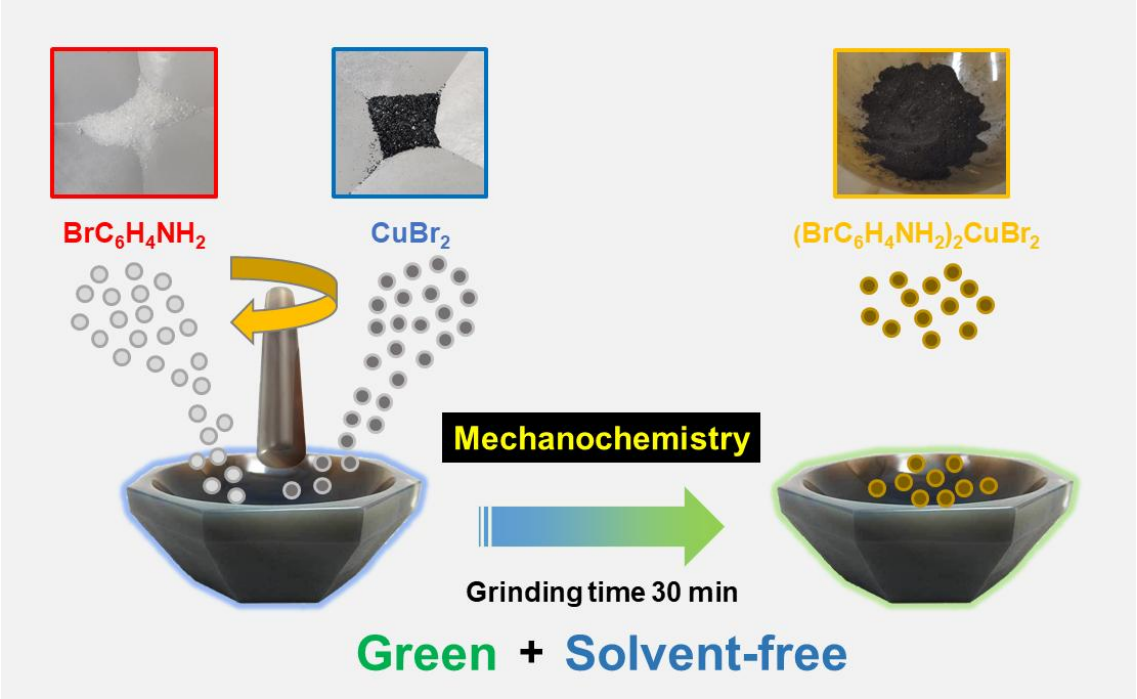

Fig. S2 Illustration of the synthesis of (Br-C_6H_4-NH_2)$_2$$CuBr_2$ powders via a mechanochemistry method. The (Br-C_6H_4-NH_2)$_2$$CuBr_2$ powders were fabricated by grinding the mixture of Br-C_6H_4-NH_2 and $CuBr_2$ powders with a molar ratio of 2:1 in a mortar for 30 min. Then, the powders were heated at 50 °C for 30 min to promote the chemical reaction. Finally, to prevent the residue of the reactant remaining in the mixture, the powders were ground for 10 min. Then, black (Br-C_6H_4-NH_2)$_2$$CuBr_2$ powders were obtained.

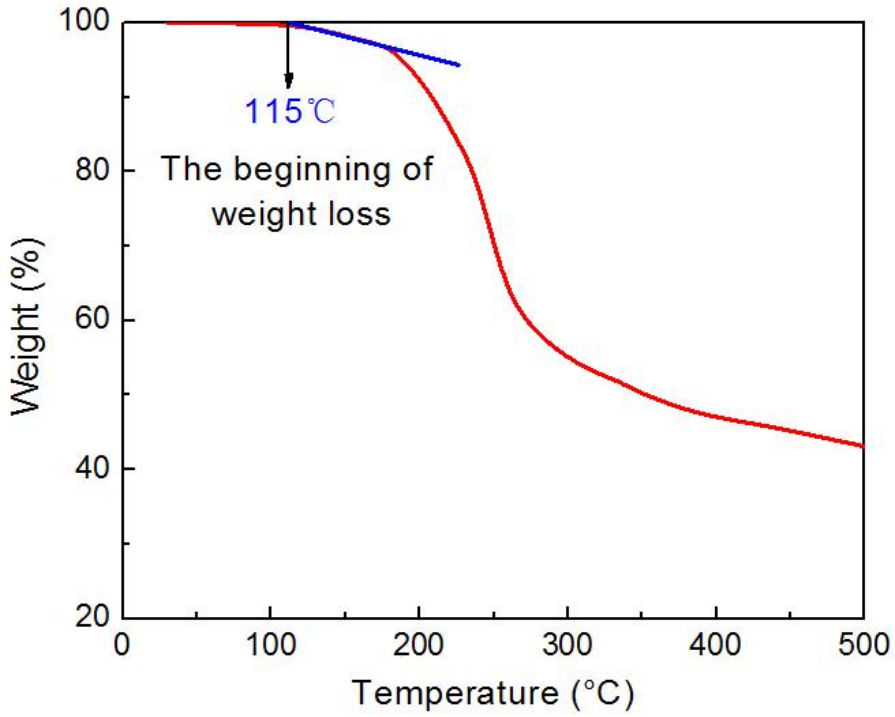

Fig. S3 Thermo gravimetric analysis curve of $(Br\text{-}C_6H_4\text{-}NH_2)_2CuBr_2$ powders obtained via a mechanochemistry method.

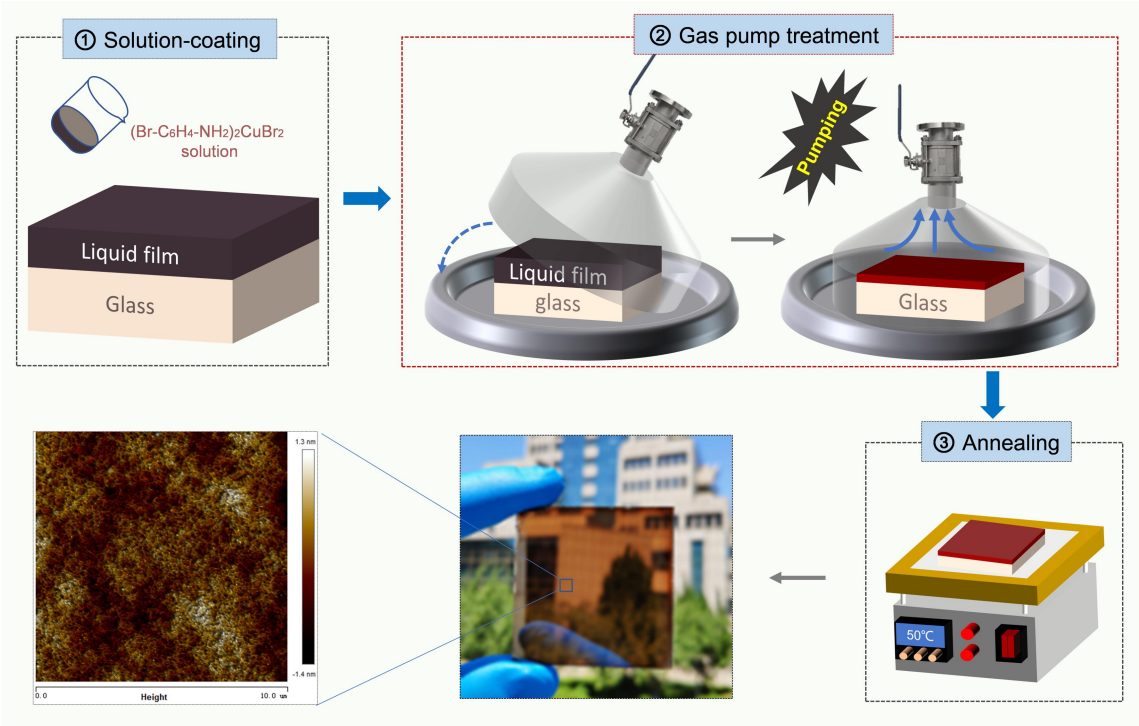

Fig. S4 Gas pump treatment procedure for preparing a $(Br\text{-}C_6H_4\text{-}NH_2)_2CuBr_2$ film.

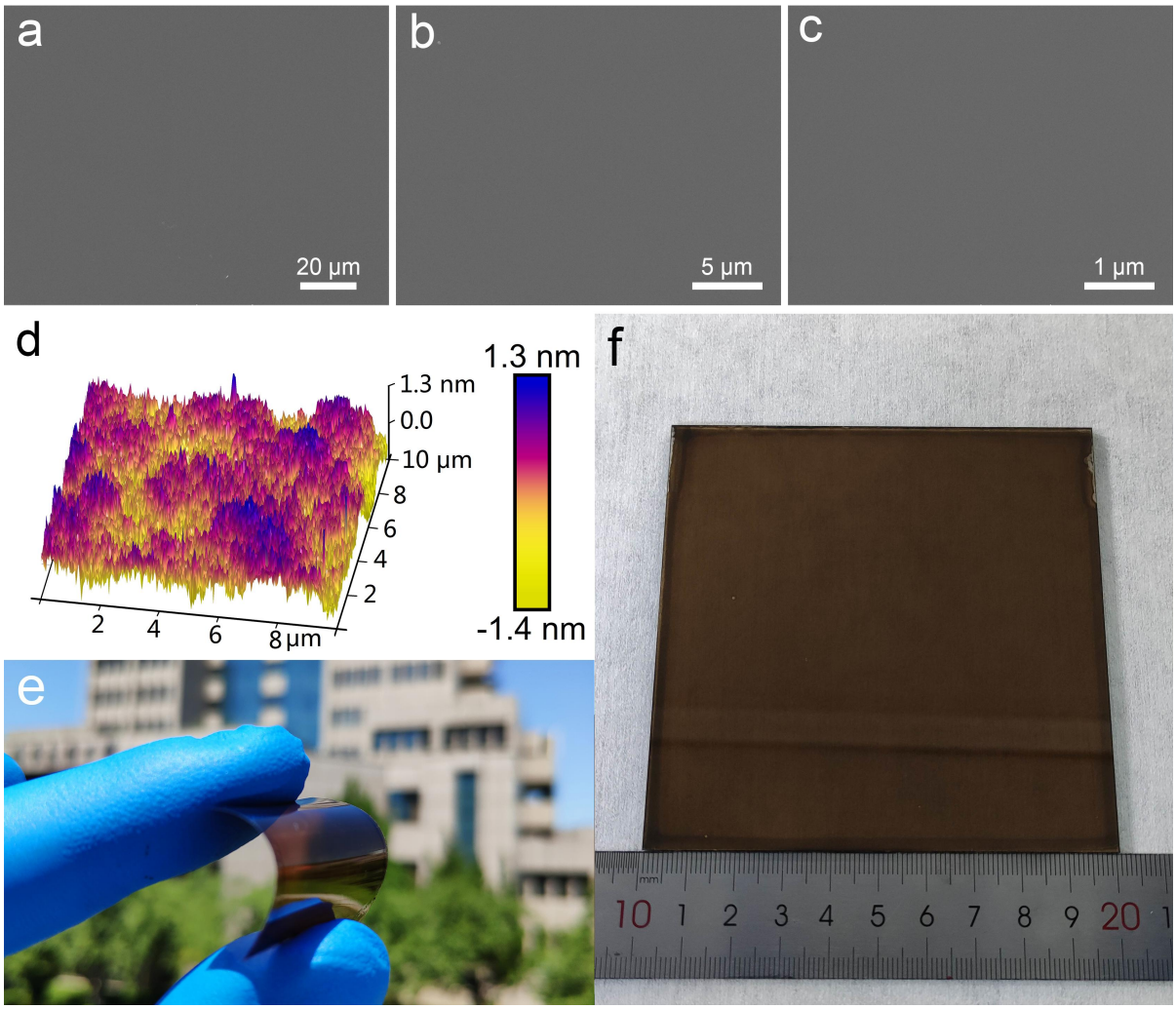

Fig. S5 (a-c) SEM images of the $(Br\text{-}C_6H_4\text{-}NH_2)_2CuBr_2$ film at different magnifications. d. High-resolution 3D image atomic force microscopy of $(Br\text{-}C_6H_4\text{-}NH_2)_2CuBr_2$ film. e. A photograph of one $(Br\text{-}C_6H_4\text{-}NH_2)_2CuBr_2$ film deposited on flexible PET/ITO substrate. f. Photographs of large-area (100 cm^2) $(Br\text{-}C_6H_4\text{-}NH_2)_2CuBr_2$ films.

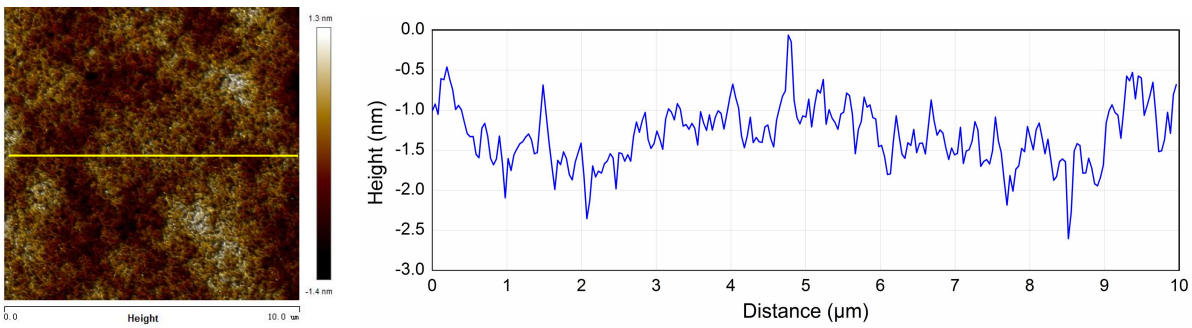

Fig. S6 A two-dimentional topographic AFM image (left) and its surface cross-sectional profile (right) of one $(Br\text{-}C_6H_4\text{-}NH_2)_2CuBr_2$ film along the yellow line.

Fig. S7 A cross-sectional SEM micrograph of one $(Br\text{-}C_6H_4\text{-}NH_2)_2CuBr_2$ film.

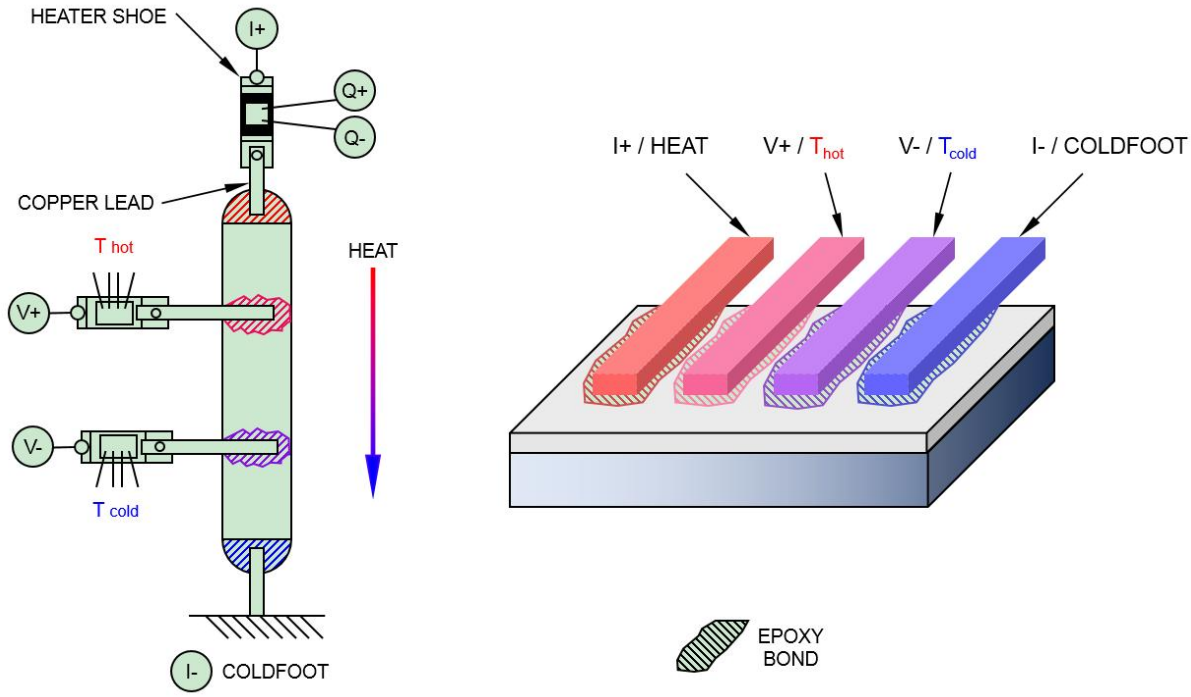

Fig. S8 Schematic diagram of the measurements of thermoelectric properties via PPMS. Thermal and electrical connections foran idealized sample (left) and a real film sample (right). The sample is shown mounted in the four probe geometry.

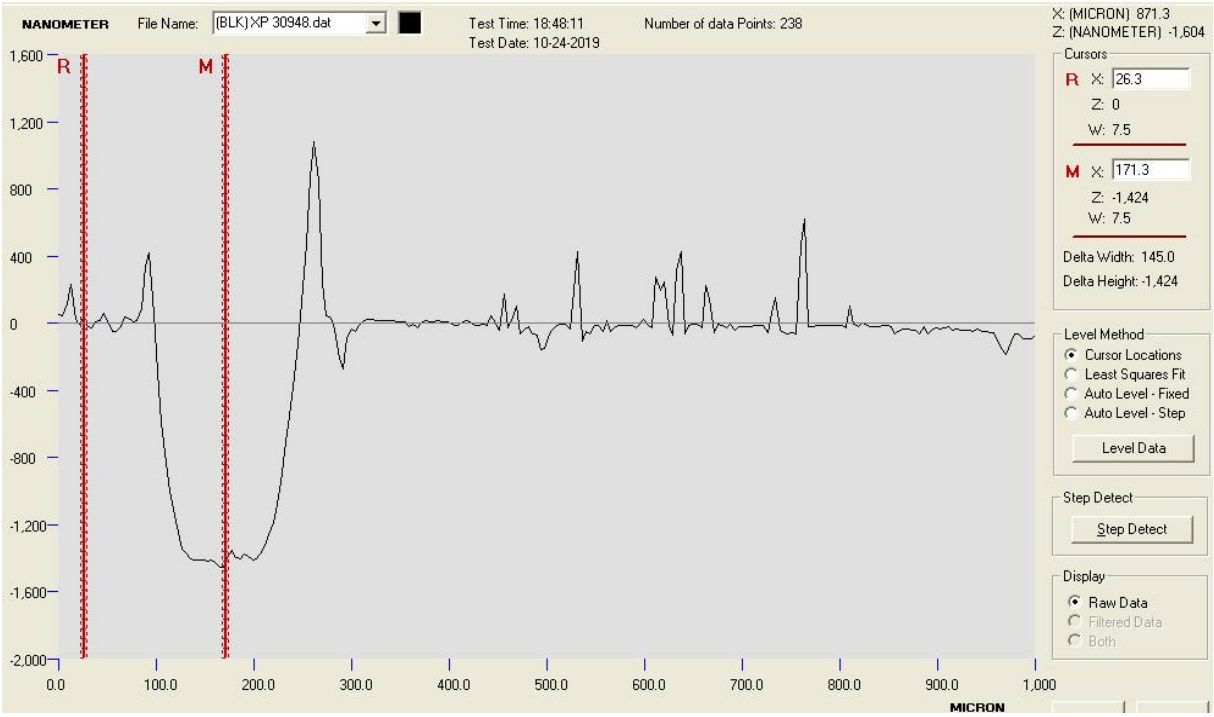

Fig. S9 Thickness measurement data of the $(Br\text{-}C_6H_4\text{-}NH_2)_2CuBr_2$ film.

Table S1 Thermoelectric properties of one sample tested for 20 times at 298 K.

Number	*PF* ($\mu W\ K^{-2}\ m^{-1}$)	*S* ($\mu V\ K^{-1}$)	*ZT*	κ ($W\ K^{-1}\ m^{-1}$)	σ ($S\ cm^{-1}$)
1	1589.116236	−63.10078487	0.126152272	3.753886609	3991.040569
2	1589.245165	−63.10350015	0.126296403	3.749738743	3991.020892
3	1588.868729	−63.09662036	0.126254473	3.750029543	3990.945730
4	1588.915080	−63.09687960	0.125906668	3.760733193	3991.029359
5	1588.917005	−63.09674106	0.125698232	3.767062753	3991.051721
6	1588.613438	−63.09108285	0.125712198	3.765820881	3991.004975
7	1589.038188	−63.09944012	0.126160695	3.753329445	3991.014659
8	1589.097412	−63.10103124	0.126082597	3.756028246	3990.962128
9	1588.465684	−63.08810366	0.125575943	3.769543443	3991.010685
10	1589.268066	−63.10415357	0.126122252	3.754920726	3990.995751
11	1589.278029	−63.10380117	0.125931005	3.761052019	3991.065344
12	1588.582261	−63.09069278	0.125608393	3.768667925	3990.976001
13	1589.058084	−63.09996890	0.125987018	3.758759390	3990.997738
14	1589.075576	−63.10004383	0.126143980	3.754039276	3991.032192
15	1588.776733	−63.09399297	0.125608766	3.769340041	3991.047025
16	1588.617259	−63.09085715	0.125905400	3.760387580	3991.043129
17	1588.569022	−63.09042071	0.125532834	3.771061318	3990.977159
18	1589.422415	−63.10735613	0.125995484	3.759199075	3990.978257
19	1588.752743	−63.09342435	0.125939392	3.759363850	3991.058699
20	1589.275539	−63.10413403	0.125851336	3.763193093	3991.016988
Average	1588.948±0.283	−63.098±0.006	0.126±0.0002	3.760±0.007	3991.013±0.034

Table S2 Thermoelectric properties of one sample tested for 20 times at 313 K.

Number	*PF* ($\mu W\ K^{-2}\ m^{-1}$)	*S* ($\mu V\ K^{-1}$)	*ZT*	κ ($W\ K^{-1}\ m^{-1}$)	σ ($S\ cm^{-1}$)
1	1693.775103	−67.61317644	0.145899093	3.633636175	3705.041408
2	1693.622191	−67.61052016	0.145452828	3.644460191	3704.998028
3	1693.098416	−67.59970207	0.145753265	3.635760507	3705.037771
4	1692.694151	−67.59221205	0.145030091	3.653177489	3704.974083
5	1693.261135	−67.60303059	0.145255824	3.648721961	3705.028980
6	1693.513301	−67.60764321	0.145628695	3.639944977	3705.075126
7	1692.781487	−67.59376104	0.145228059	3.648546597	3704.99543
8	1693.395751	−67.60604070	0.145994527	3.630416563	3704.993587
9	1693.235825	−67.60301559	0.145324310	3.646934794	3704.975244
10	1693.539899	−67.60909123	0.145596241	3.640703149	3704.974609
11	1692.864335	−67.59536479	0.145113609	3.651268672	3705.000945
12	1693.396826	−67.60585828	0.145603890	3.640411200	3705.015935
13	1693.655657	−67.61154351	0.145413456	3.645511795	3704.959082
14	1692.753320	−67.59305425	0.145579257	3.639501173	3705.011264
15	1693.373886	−67.60556526	0.145639948	3.639348401	3704.997861
16	1692.778118	−67.59379104	0.145342220	3.645518827	3704.984768
17	1692.512003	−67.58805980	0.145149056	3.649863548	3705.030589
18	1692.917508	−67.59653114	0.145344459	3.645655749	3704.989461
19	1692.808314	−67.59515983	0.145357071	3.645119121	3704.900806
20	1692.942124	−67.59676654	0.145943000	3.630873732	3705.017528
Average	1693.146±0.376	−67.601±0.007	0.145±0.0003	3.643±0.007	3705.000±0.036

Table S3 Thermoelectric properties of one sample tested for 20 times at 328 K.

Number	*PF* ($\mu W\ K^{-2}\ m^{-1}$)	*S* ($\mu V\ K^{-1}$)	*ZT*	κ ($W\ K^{-1}\ m^{-1}$)	σ ($S\ cm^{-1}$)
1	1789.137222	−71.71240029	0.166333447	3.528025375	3479.005642
2	1788.267455	−71.69515622	0.165423512	3.545791559	3478.987290
3	1789.305479	−71.71602247	0.165674683	3.542523575	3478.981365
4	1788.505871	−71.70034422	0.166396209	3.525535074	3478.947610
5	1788.714469	−71.70455209	0.166161584	3.530740275	3478.945022
6	1788.117371	−71.69194283	0.166020289	3.532817928	3479.007161
7	1788.686386	−71.70343618	0.165901021	3.536279975	3478.998684
8	1788.208120	−71.69380264	0.165821322	3.537060850	3479.003220
9	1788.324200	−71.69661819	0.165293062	3.548625500	3478.955800
10	1788.290371	−71.69581055	0.165265124	3.549296345	3478.968369
11	1789.048239	−71.71080327	0.166129347	3.532157187	3478.987563
12	1789.106804	−71.71136652	0.166794847	3.518087425	3479.046797
13	1787.660447	−71.68277826	0.165408049	3.545101927	3479.007563
14	1788.475055	−71.69889007	0.166334002	3.526754720	3479.028783
15	1788.144500	−71.69260611	0.165944660	3.534332101	3478.995568
16	1788.489886	−71.69966151	0.164781794	3.559963094	3478.982770
17	1788.486524	−71.69937746	0.165233618	3.550241898	3479.003794
18	1789.703079	−71.72362250	0.165319781	3.550841283	3479.017018
19	1789.141608	−71.71277168	0.166014377	3.534896007	3478.978135
20	1788.888079	−71.70750013	0.166218124	3.530014009	3478.996608
Average	1788.635±0.494	−71.702±0.010	0.166±0.0005	3.538±0.011	3478.992±0.026

Table S4 Thermoelectric properties of one sample tested for 20 times at 343 K.

Number	*PF* ($\mu W\ K^{-2}\ m^{-1}$)	*S* ($\mu V\ K^{-1}$)	*ZT*	κ ($W\ K^{-1}\ m^{-1}$)	σ ($S\ cm^{-1}$)
1	1804.110784	−76.45956837	0.183354275	3.374897861	3086.025558
2	1803.841850	−76.45426834	0.183156094	3.378036464	3085.993348
3	1804.350560	−76.46507514	0.183046005	3.380972456	3085.991172
4	1804.865810	−76.47624389	0.182939562	3.384191635	3085.970848
5	1804.071701	−76.45905378	0.182952182	3.382418143	3086.000243
6	1803.519702	−76.44776494	0.182645821	3.386971281	3085.967198
7	1804.970410	−76.47799517	0.182733335	3.387979088	3086.008354
8	1804.898528	−76.47608398	0.182581057	3.390631468	3086.039695
9	1804.328962	−76.46427357	0.182584371	3.389573941	3086.018934
10	1803.988583	−76.45703900	0.182975889	3.381732613	3086.020701
11	1803.967301	−76.45708033	0.183106144	3.379219002	3085.980959
12	1803.856449	−76.45430097	0.182623420	3.387924307	3086.015690
13	1804.461939	−76.46848178	0.182917115	3.383737422	3085.906695
14	1803.968614	−76.45651931	0.182595969	3.388568226	3086.028493
15	1804.331005	−76.46387949	0.182405342	3.392840764	3086.054238
16	1804.456194	−76.46725566	0.182403394	3.393304068	3085.995834
17	1804.283581	−76.46373455	0.182590515	3.389336225	3085.984824
18	1803.992930	−76.45783504	0.182160622	3.396913825	3085.963879
19	1803.909989	−76.45558345	0.183454030	3.372818792	3086.003753
20	1804.098298	−76.45958812	0.182297600	3.394465487	3086.002606
Average	1804.214±0.380	−76.462±0.008	0.183±0.0003	3.386±0.007	3085.999±0.032

Table S5 Thermoelectric properties of one sample tested for 20 times at 358 K.

Number	*PF* ($\mu W K^{-2} m^{-1}$)	*S* ($\mu V K^{-1}$)	*ZT*	κ ($W K^{-1} m^{-1}$)	σ ($S cm^{-1}$)
1	1970.289090	−82.24261641	0.218710034	3.225001081	2912.970699
2	1970.793134	−82.25287258	0.218807596	3.224572736	2912.989321
3	1971.642835	−82.26985151	0.219203122	3.220096222	2913.042480
4	1971.259422	−82.26287528	0.219392458	3.216617448	2912.970000
5	1970.685812	−82.25014382	0.218662978	3.226565973	2913.023967
6	1970.599521	−82.24948383	0.219325095	3.216537147	2912.943161
7	1970.695194	−82.25139979	0.218810547	3.224258559	2912.948873
8	1970.917033	−82.25549305	0.218403395	3.230555184	2912.986842
9	1970.466736	−82.24582692	0.219514746	3.213468256	2913.005904
10	1970.616030	−82.24854315	0.217791092	3.239296521	2913.034198
11	1971.022132	−82.25712748	0.218704541	3.226302066	2913.026411
12	1971.240393	−82.26186860	0.218682346	3.227050461	2913.013175
13	1970.877924	−82.25393962	0.218466305	3.229506814	2913.039067
14	1970.817331	−82.25335377	0.218258171	3.232524916	2912.991002
15	1970.453396	−82.24564359	0.218414813	3.229684624	2912.999169
16	1970.383270	−82.24397481	0.219690394	3.210931993	2913.013710
17	1971.105880	−82.25878408	0.218472438	3.229940834	2913.032851
18	1970.751017	−82.25188472	0.219060305	3.220703649	2912.997038
19	1970.247184	−82.24162414	0.218273072	3.231493543	2912.979034
20	1970.613386	−82.24900828	0.219933509	3.207812302	2912.997341
Average	1970.774±0.353	−82.252±0.007	0.219±0.0005	3.224±0.008	2913.000±0.029

Table S6 Thermoelectric properties of one sample tested for 20 times at 373 K.

Number	*PF* ($\mu W\ K^{-2}\ m^{-1}$)	*S* ($\mu V\ K^{-1}$)	*ZT*	κ ($W\ K^{-1}\ m^{-1}$)	σ ($S\ cm^{-1}$)
1	2003.719619	−84.97356900	0.245645148	3.042473680	2775.039896
2	2003.596785	−84.97098994	0.246379359	3.033469654	2775.038229
3	2003.271414	−84.96517481	0.245223309	3.046987800	2774.967387
4	2003.184724	−84.96348976	0.246239741	3.034410736	2774.957368
5	2003.126089	−84.96123927	0.244405355	3.056993437	2775.023149
6	2003.455833	−84.96883586	0.245304620	3.04640722	2774.983700
7	2004.417036	−84.98826355	0.246694869	3.030692921	2775.045916
8	2002.969819	−84.95884456	0.245595160	3.042074573	2774.963088
9	2003.687323	−84.97341603	0.248367282	3.009209998	2775.005160
10	2003.230679	−84.96514009	0.245655732	3.041631938	2774.913227
11	2003.767544	−84.97536574	0.245755907	3.041193923	2774.988916
12	2003.681333	−84.97357198	0.246151270	3.036303485	2774.986679
13	2002.611483	−84.95082386	0.246147707	3.034654200	2774.990572
14	2003.461583	−84.96820530	0.245997226	3.037882131	2775.032852
15	2003.857210	−84.97711594	0.246828016	3.028103466	2774.998782
16	2003.655088	−84.97329558	0.246025938	3.037651519	2774.968383
17	2003.370486	−84.96775284	0.245340113	3.045881101	2774.936224
18	2003.500923	−84.96957587	0.246159064	3.035896604	2774.997817
19	2003.108695	−84.96164133	0.246431697	3.031897662	2774.972787
20	2003.289975	−84.96557836	0.246048807	3.036996185	2774.966738
Average	2003.448±0.383	−84.969±0.008	0.246±0.0008	3.038±0.009	2774.989±0.035

Table S7 Thermoelectric properties of one sample tested for 20 times at 388 K.

Number	PF ($\mu W\ K^{-2}\ m^{-1}$)	S ($\mu V\ K^{-1}$)	ZT	κ ($W\ K^{-1}\ m^{-1}$)	σ ($S\ cm^{-1}$)
1	2026.650944	−88.15317234	0.268968895	2.923600543	2607.972838
2	2026.695078	−88.15311655	0.268800887	2.925419993	2608.032932
3	2027.524050	−88.17162944	0.268264336	2.932452100	2608.004166
4	2027.393116	−88.16959698	0.270236552	2.910872457	2607.955977
5	2026.642068	−88.15282779	0.268528497	2.928316923	2607.981802
6	2027.662698	−88.17500817	0.268427807	2.930966049	2607.982630
7	2026.828929	−88.15601129	0.269947556	2.913190558	2608.033891
8	2027.035679	−88.16010431	0.267839384	2.936498529	2608.057742
9	2026.403813	−88.14769639	0.269230980	2.920325577	2607.978818
10	2026.722753	−88.15449163	0.267195553	2.943208637	2607.987182
11	2026.565898	−88.15147947	0.269004635	2.922891073	2607.963562
12	2026.834506	−88.15538978	0.269102449	2.922279605	2608.077841
13	2027.230346	−88.16505011	0.269891675	2.914413597	2608.015579
14	2026.717940	−88.15331848	0.268861120	2.924733041	2608.050403
15	2027.052372	−88.16221999	0.268425474	2.929949743	2607.954046
16	2027.122151	−88.16383888	0.267988483	2.934784436	2607.948043
17	2026.837347	−88.15685495	0.269169806	2.921659571	2607.994806
18	2026.713749	−88.15391905	0.269585196	2.917023263	2608.009474
19	2026.473569	−88.14864047	0.267688147	2.937306842	2608.012729
20	2027.009706	−88.16045989	0.267964838	2.935023185	2608.003286
Average	2026.906±0.344	−88.158±0.008	0.269±0.0008	2.926±0.009	2608.001±0.036

.

Table S8 Summary of thermoelectric properties for representative n-type organic thermoelectric materials at room temperature.

Type	Materials	σ ($S\ cm^{-1}$)	*PF* ($\mu W\ m^{-1}\ K^{-2}$)	*ZT*	Reference
Conjugated polymer	FBDPPV doped with $(N\text{-}DMBI)_2$	7.2	7	—	[7]
	PDTz doped with TP-DMBI	11	15	—	[8]
	P(PzDPP-CT2) doped with N-DMBI	6.0	57.3	—	[9]
	ClBDPPV doped with TBAF	0.62	0.63	—	[10]
	PNDTI-BTT-PD doped with N-DMBI	5	14	—	[11]
	PNDIClTVT doped with NDI-TBAF	0.2	67	—	[12]
	P(PymPh) doped with NaNap	18	0.485	—	[13]
	PDPF doped with 5wt% N-DMBI	1.3	4.65	—	[14]
Metal-organic coordination small molecular	$(Br\text{-}C_6H_4\text{-}NH_2)_2CuBr_2$	3991	1588.95	0.13	This work
	$(DMDCNQI)_2Cu$	1000	116	—	[15]
	$(DMe\text{-}DCNQI)_2Cu$	1000	110	—	[16]
	$TTF[Ni(dmit)_2]_2$ (crystal)	300	29	—	[17]
Small molecular	$(TTM\text{-}TTP)(I_3)_{5/3}$	250	76	—	[18]
	Bi-doped TDPPQ	3.3	113	—	[19]
	PTEG-2	8.35	46	0.15	[20]
	PTEG-1 doped with N-DMBI	2.05	16.7	—	[21]
	2DQTT-*o*-OD doped with $(2\text{-}Cyc\text{-}DMBI\text{-}Me)_2$	N/A	17.2	0.02	[22]
	C60 doped with Cs_2CO_3	8.6	20.5	—	[23]
	PCBM doped with N-DMBI	40	35	—	[24]
	PCBM doped with AOB and N-DMBI	2	1	—	[25]
	TTF-TCNQ (crystal)	500	39.2	—	[26]
	PDI-3	0.5	1.4	—	[27]
	2DQQT-Se	0.29	1.4	—	[28]
	Q-DCM-DPPTT doped with N-DMBI	0.11	1.7	—	[29]
	A-DCV-DPPTT doped with N-DMBI	3.1	105	0.11	[29]
	2DQQT doped with N-DMBI	14	41.6	0.03	[30]
Metal-organic coordination polymer	$Poly[K_x(Ni\text{-}ett)]$ film	223	453	0.21	[31]
	$Poly[K_x(Ni\text{-}ett)]$ compressed cuboid	45	66	0.096	[32]
	$Poly[Na_x(Ni\text{-}ett)]$ compressed cuboid	41	28	0.042	[32]

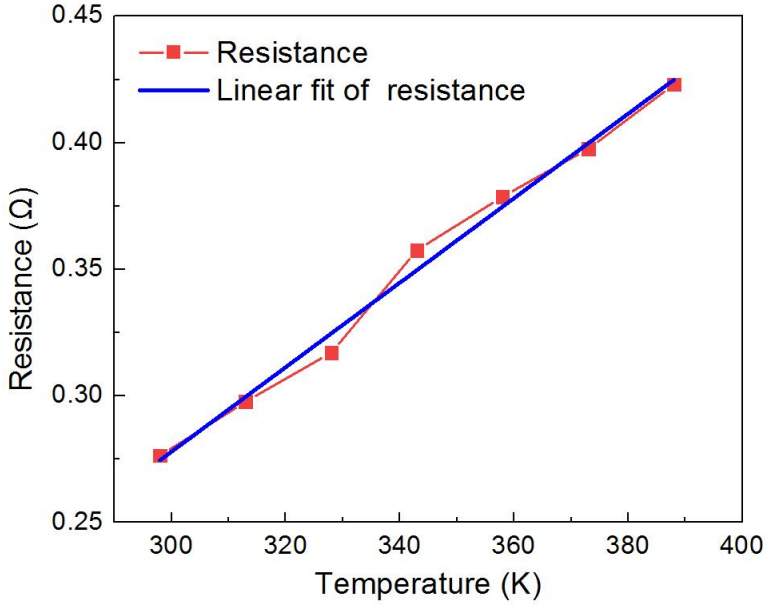

Fig. S10 Resistance at different temperature of a $(Br\text{-}C_6H_4\text{-}NH_2)_2CuBr_2$ film.

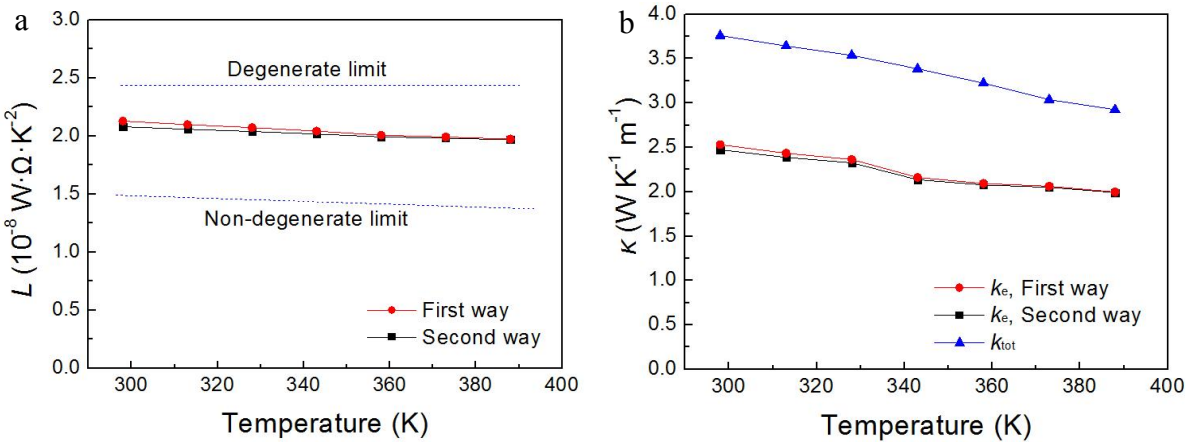

Fig. S11 (a) Lorenz number that calculated via two ways and correspondent (b) electrical thermal conductivity of $(Br\text{-}C_6H_4\text{-}NH_2)_2CuBr_2$ material.

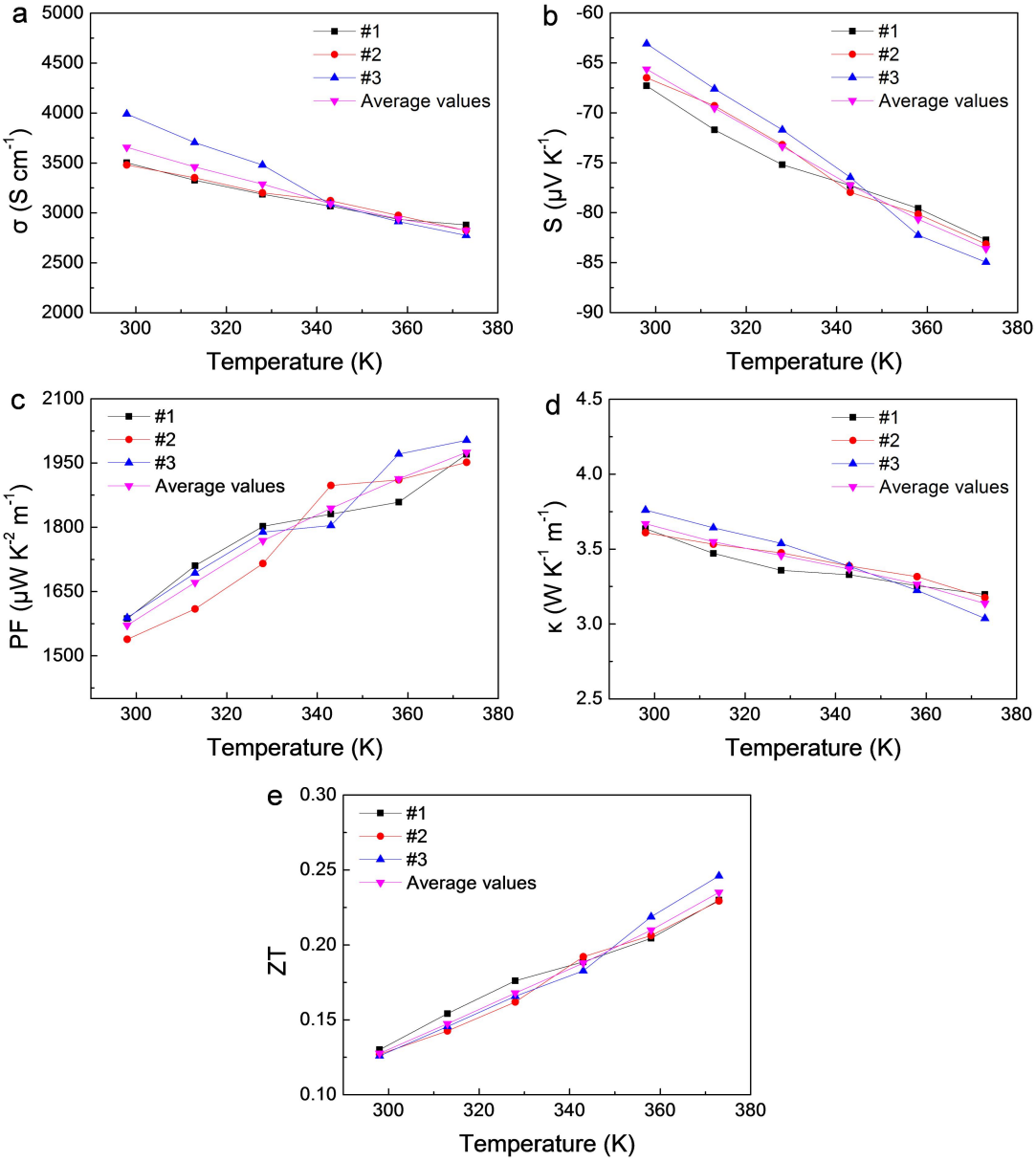

Fig. S12 The reproducibility of thermoelectric properties for three different samples tested from 298 K to 373 K. The sample #3 shows the highest performance.

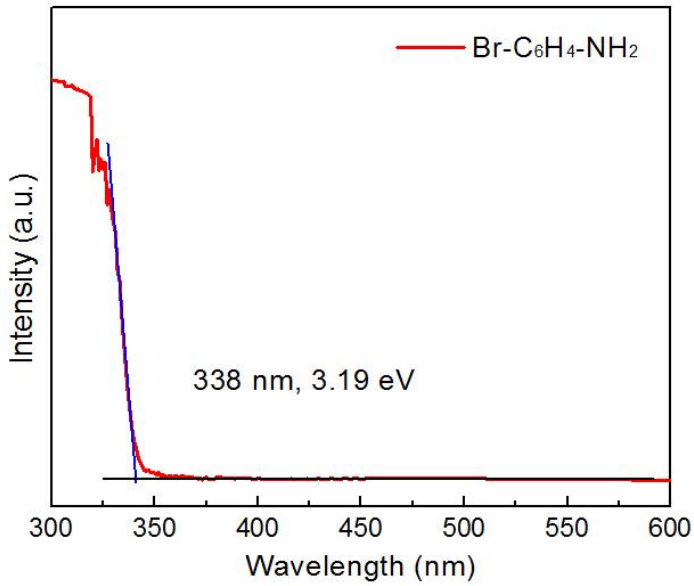

Fig. S13 UV-Vis-NIR absorption spectrum of Br-C_6H_4-NH_2 powders. The bandgap is estimated by the equation $E_g = 1240 / \lambda_{edge}$ (λ_{edge} is the threshold of absorption wavelength).

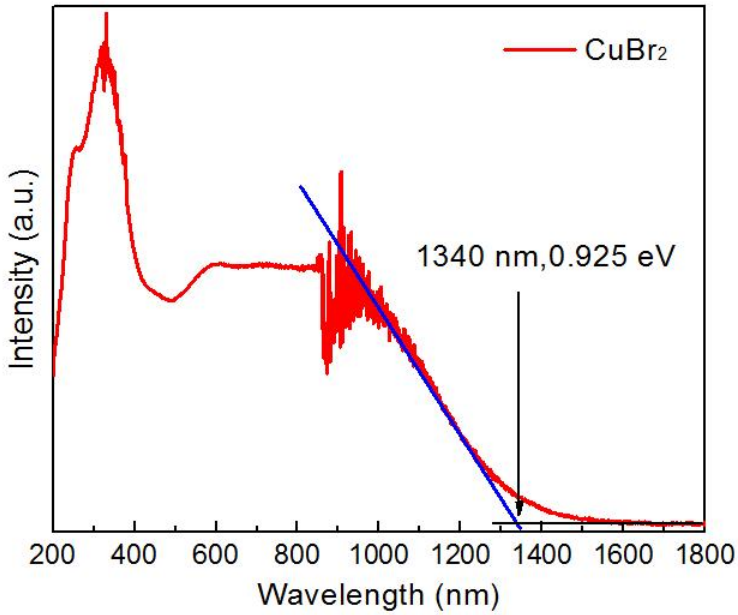

Fig. S14 UV-Vis-NIR absorption spectrum of $CuBr_2$ powders. The bandgap is estimated by the equation $E_g = 1240 / \lambda_{edge}$ (λ_{edge} is the threshold of absorption wavelength).

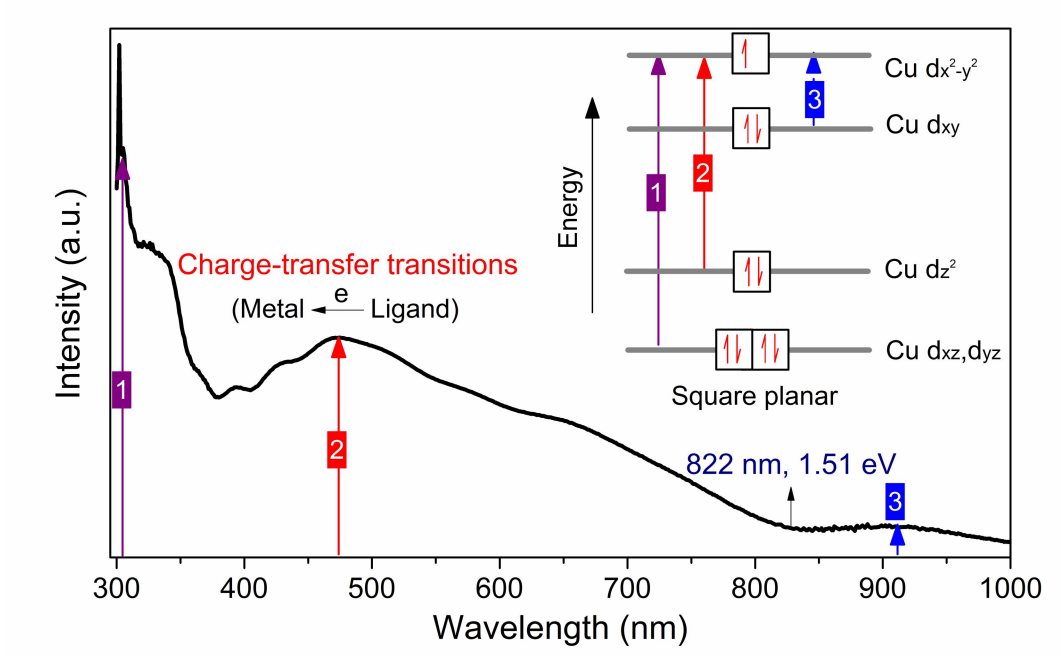

Fig. S15 UV-Vis-NIR absorption spectrum of a (Br-C_6H_4-NH_2)$_2$$CuBr_2$ film. The bandgap is estimated by the equation E_g = 1240 / λ_{edge} (λ_{edge} is the threshold of absorption wavelength). The inset is a diagram of the metal-to-ligand charge transfer (MLCT) transitions 1 and 2 for (Br-C_6H_4-NH_2)$_2$$CuBr_2$.

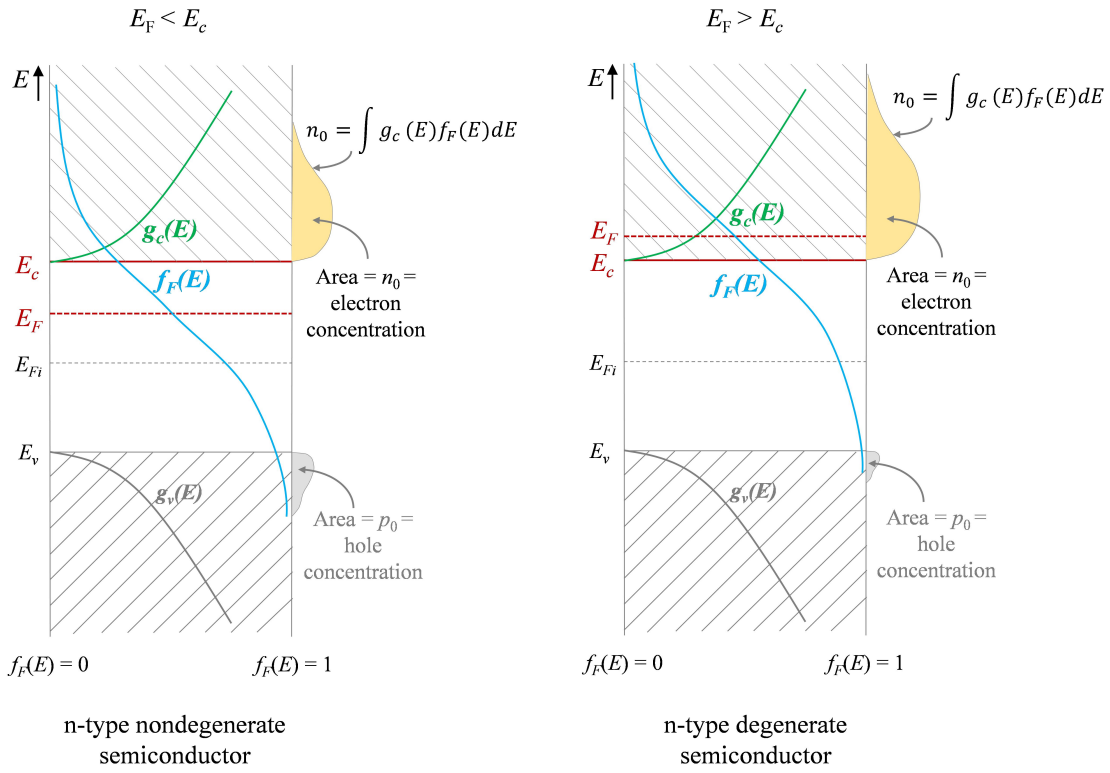

Fig. S16 Density of states functions g_c(E), Fermi-Dirac probability function f_F(E), and areas representing electron and hole concentrations for the case when E_F is above the intrinsic Fermi energy E_{Fi}.

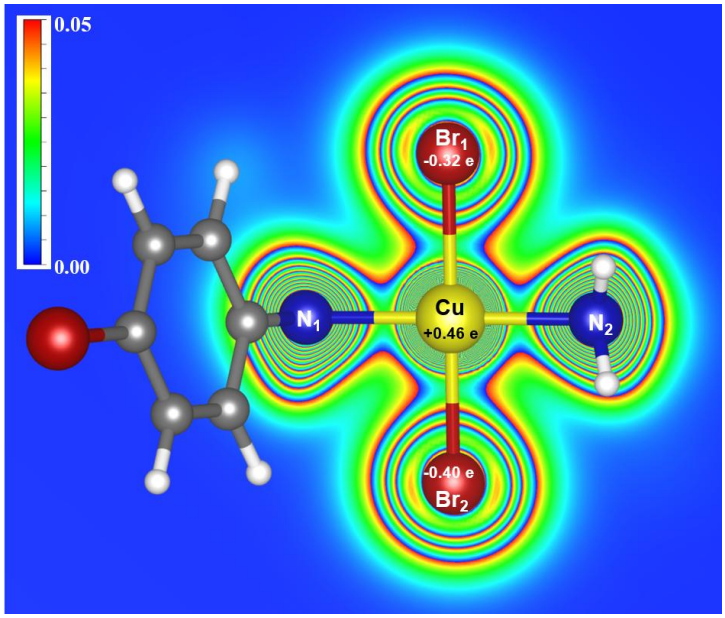

Fig. S17 Bader charge analysis and 2D charge density map for $(Br\text{-}C_6H_4\text{-}NH_2)_2CuBr_2$.

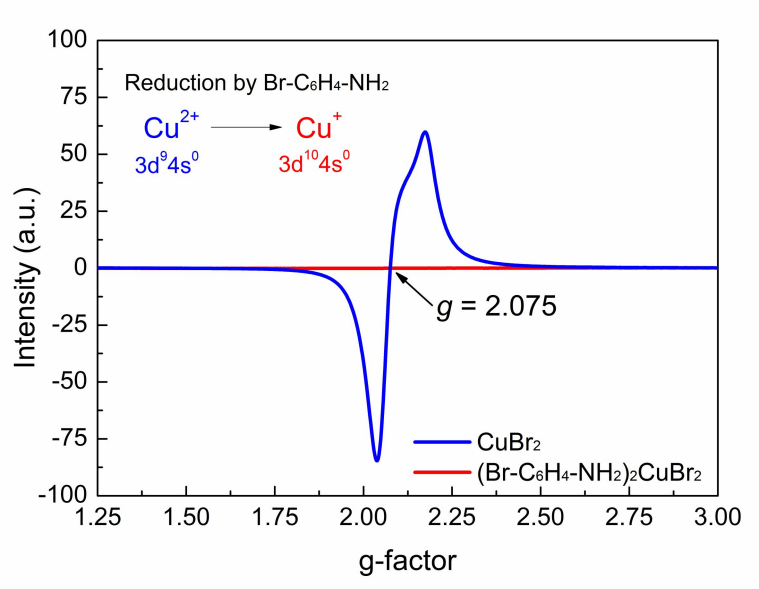

Fig. S18 Electron paramagnetic resonance (EPR) spectra of $CuBr_2$ and $(Br\text{-}C_6H_4\text{-}NH_2)_2CuBr_2$.

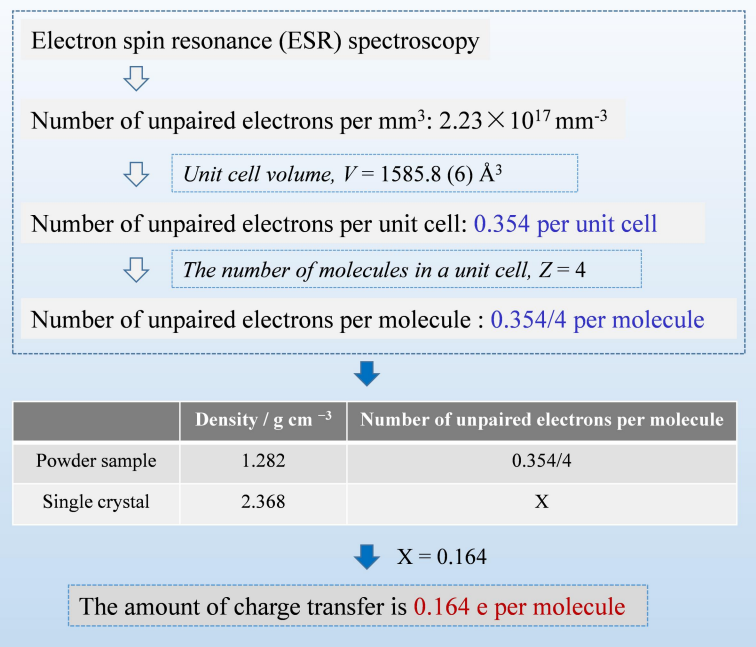

Fig. S19 The detailed calculation process of the amount of charge transfer per $(Br\text{-}C_6H_4\text{-}NH_2)_2CuBr_2$ molecule.

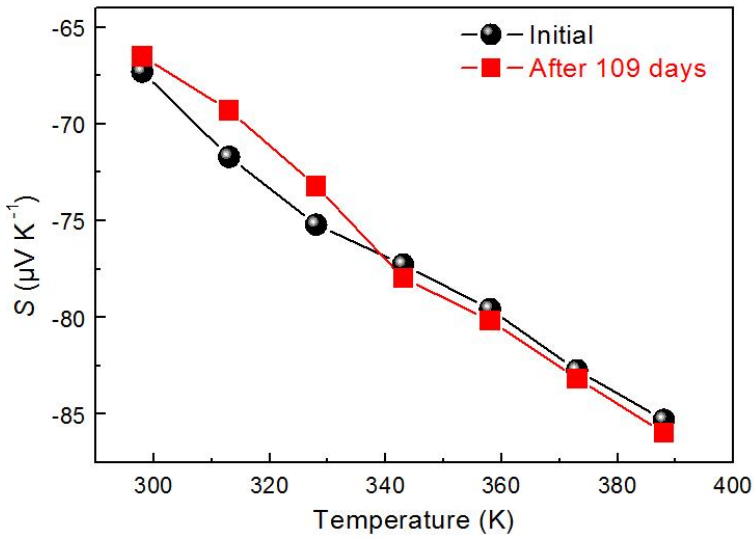

Fig. S20 Seebeck coefficient of the $(Br\text{-}C_6H_4\text{-}NH_2)_2CuBr_2$ film before and after storage in ambient air (relative humidity of 50 ± 20%, room temperature) for 109 days.

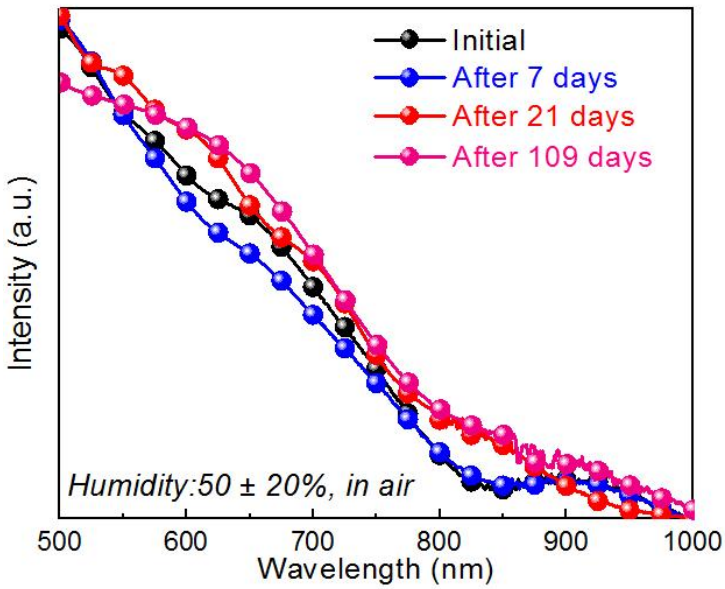

Fig. S21 UV-Vis-NIR spectra of the $(BrC_6H_4NH_2)_2CuBr_2$ film before and after storage in ambient air (relative humidity of 50 ± 20%, room temperature) for 7, 21, and 109 days.

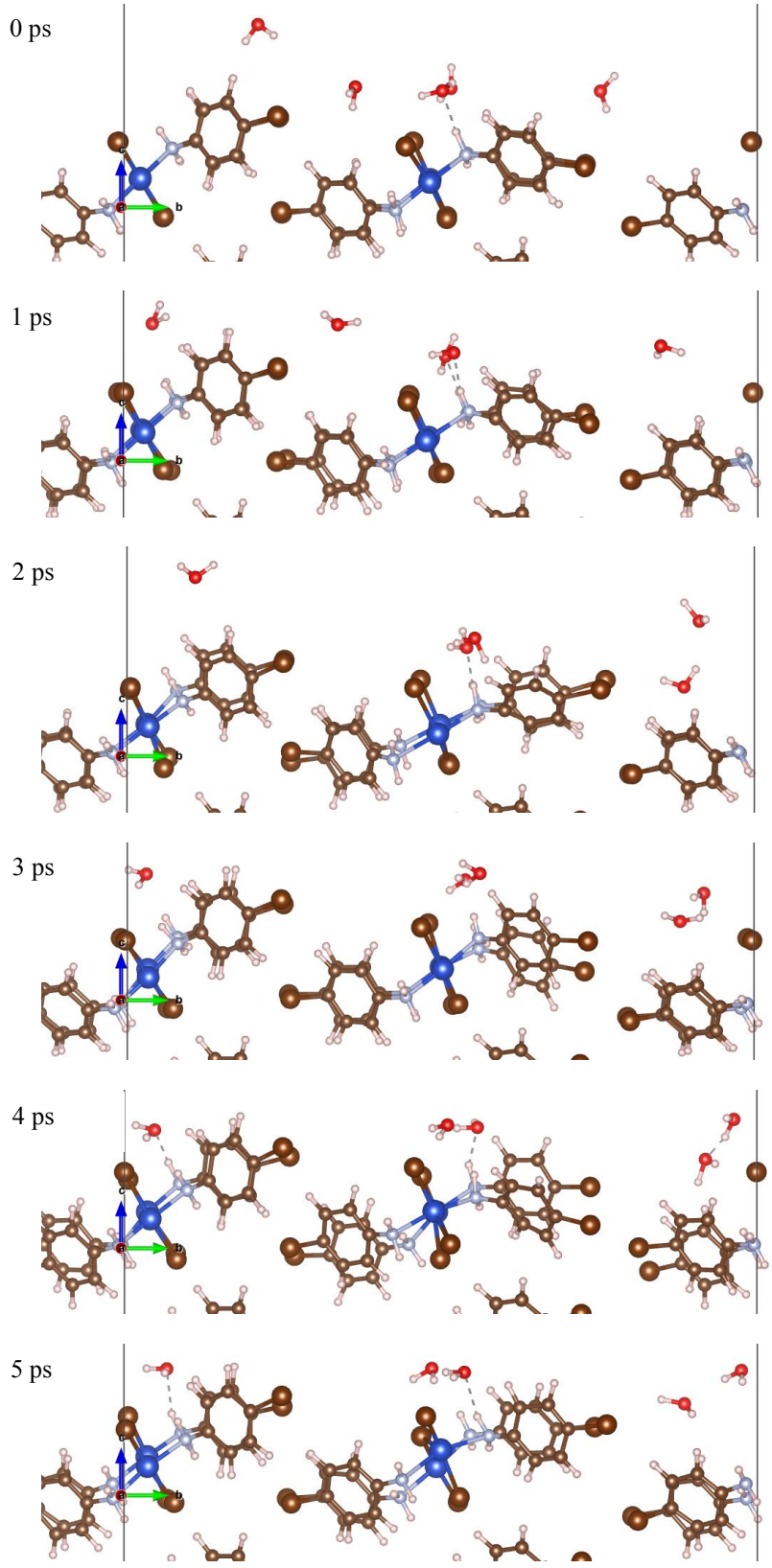

Fig. S22 Snapshots of AIMD simulation at 0, 1, 2, 3, 4, 5 ps for the $(BrC_6H_4NH_2)_2CuBr_2$ systems with five H_2O molecules. The gray dotted lines represents hydrogen bonds (N— H···O).

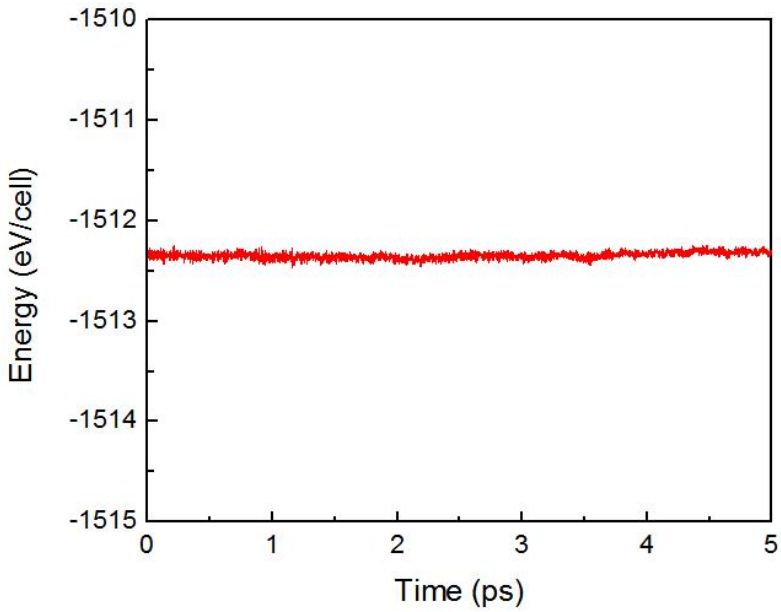

Fig. S23 The AIMD total energy of $(BrC_6H_4NH_2)_2CuBr_2$ during the heating process at 300 K from its initial configuration.

REFERENCES

1. G. Kresse, J. Hafner, *Phys. Rev. B* 1993, **47**, 558.
2. G. Kresse, J. Furthmuller, *Phys. Rev*. B 1996, **54**, 11169.
3. G. Kresse, D. Joubert, *Phys. Rev. B* 1999, **59**, 1758–1775.
4. D. M. Rowe, C. M. Bhandari. Modern Thermoelectrics, Holt, Rinehart and Winston, 1993.
5. W.-T. Chiu, C.-L. Chen and Y.-Y. Chen, *Sci. Rep.*, 2016, **6**, 23143.
6. H.-S. Kim, Z. M. Gibbs, Y. Tang, H. Wang and G. J. Snyder, *APL Mater.*, 2015, **3**, 041506.
7. H.I. Un, S.A. Gregory, S.K. Mohapatra, M. Xiong, E. Longhi, Y. Lu, S. Rigin, S. Jhulki, C.Y. Yang, T.V. Timofeeva, et al. *Adv. Energy Mater*. 2019, **9**, 1900817.
8. J. Han, A. Chiu, C. Ganley, P. McGuiggan, S.M. Thon, P. Clancy, and H.E. Katz, *Angew. Chem. Int. Ed.* 2021, **60**, 27212.
9. X. Yan, M. Xiong, J.T. Li, S. Zhang, Z. Ahmad, Y. Lu, Z.Y. Wang, Z.F. Yao, J.Y. Wang, X. Gu, and T. Lei, *J. Am. Chem. Soc*. 2019, **141**, 20215–20221.
10. X. Zhao, D. Madan, Y. Cheng, J. Zhou, H. Li, S.M. Thon, A.E. Bragg, M.E. DeCoster, P.E. Hopkins, and H.E. Katz, *Adv. Mater*. 2017, **29**, 1606928.
11. Y. Wang, M. Nakano, T. Michinobu, Y. Kiyota, T. Mori, and K. Takimiya, *Macromolecules* 2017, **50**, 857–864.
12. J. Han, C. Ganley, Q. Hu, X. Zhao, P. Clancy, T.P. Russell, and H.E. Katz, *Adv. Funct. Mater*. 2021, **31**, 2010567.
13. S. Hwang, W.J. Potscavage, Y.S. Yang, I.S. Park, T. Matsushima, and C. Adachi, *Phys. Chem. Chem. Phys.* 2016, **18**, 29199–29207.
14. C.Y. Yang, W.L. Jin, J. Wang, Y.F. Ding, S. Nong, K. Shi, Y. Lu, Y.Z. Dai, F.D. Zhuang, T. Lei, et al.

Adv. Mater. 2018, **30**, 1802850.

15. T. Mori, H. Inokuchi, A. Kobayashi, R. Kato, and H. Kobayashi, *Phys. Rev. B. Condens. Matter.* 1988, **38**, 5913–5923.
16. F. Huewe, A. Steeger, K. Kostova, L. Burroughs, I. Bauer, P. Strohriegl, V. Dimitrov, S. Woodward, and J. Pflaum, *Adv. Mater*. 2017, **29**, 1605682.
17. R. Sato, Y. Kiyota, T. Kadoya, T. Kawamoto, and T. Mori, *RSC Adv*. 2016, **6**, 41040–41044.
18. T. Mori, Y. Misaki, and T. Yamabe, *Bull. Chem. Soc. Jpn*. 1997, **70**, 1809–1812.
19. D. Huang, C. Wang, Y. Zou, X. Shen, Y. Zang, H. Shen, X. Gao, Y. Yi, W. Xu, C.A. Di, and D. Zhu, *Angew. Chem. Int. Ed*. 2016, ***55***, 10672–10675.
20. J. Liu, B. van der Zee, R. Alessandri, S. Sami, J. Dong, M. I. Nugraha, A. J. Barker, S. Rousseva, L. Qiu, X. Qiu, N. Klasen, R. C. Chiechi, D. Baran, M. Caironi, T. D. Anthopoulos, G. Portale, R. W. A. Havenith, S. J. Marrink, J. C. Hummelen and L. J. A. Koster, *Nat. Commun*. 2020, **11**, 5694.
21. J. Liu, L. Qiu, G. Portale, M. Koopmans, G. Ten Brink, J.C. Hummelen, and L.J.A. Koster, *Adv. Mater.* 2017, **29**, 1701641.
22. D. Yuan, D. Huang, C. Zhang, Y. Zou, C.A. Di, X. Zhu, and D. Zhu, *ACS Appl. Mater. Interfaces* 2017, ***9***, 28795–28801.
23. M. Sumino, K. Harada, M. Ikeda, S. Tanaka, K. Miyazaki, and C. Adachi, *Appl. Phys. Lett*. 2011, **99**, 093308.
24. G. Zuo, Z. Li, E. Wang, and M. Kemerink, *Adv. Electron. Mater*. 2018, **4**, 1700501.
25. F. Gao, Y. Liu, Y. Xiong, P. Wu, B. Hu, and L. Xu, *Front. Optoelectron*. 2017, **10**, 117–123.
26. P.M. Chaikin, R.L. Greene, S. Etemad, and E. Engler, *Phys. Rev. B* 1976, **13**, 1627–1632.
27. B. Russ, M.J. Robb, F.G. Brunetti, P.L. Miller, E.E. Perry, S.N. Patel, V. Ho, W.B. Chang, J.J. Urban, M.L. Chabinyc, et al. *Adv. Mater*. 2014, **26**, 3473–3477.
28. D. Yuan, Y. Guo, Y. Zeng, Q. Fan, J. Wang, Y. Yi and X. Zhu, *Angew. Chem. Int. Ed*. 2019, **58**, 4958–4962.
29. D. Huang, H. Yao, Y. Cui, Y. Zou, F. Zhang, C. Wang, H. Shen, W. Jin, J. Zhu, Y. Diao, W. Xu, C. A. Di and D. Zhu, *J. Am. Chem. Soc*. 2017, **139**, 13013–13023.
30. D. Yuan, D. Huang, S.M. Rivero, A. Carreras, C. Zhang, Y. Zou, X. Jiao, C.R. McNeill, X. Zhu, C.-a. Di, et al. *Chem* 2019, **5**, 964–976.
31. Y. Sun, L. Qiu, L. Tang, H. Geng, H. Wang, F. Zhang, D. Huang, W. Xu, P. Yue, Y. S. Guan, et al. *Adv. Mater*. 2016, **28**, 3351–3358.
32. Y. Sun, P. Sheng, C. Di, F. Jiao, W. Xu, D. Qiu and D. Zhu, *Adv. Mater.* 2012, **24**, 932–937.